Accessible Digital Ophthalmoscopy
Based on Liquid-Lens Technology

Christos Bergeles, Pierre Berthet-Rayne, Philip McCormac,
Luis C. Garcia-Peraza-Herrera, Kosy Onyenso, Fan Cao,
Khushi Vyas, Melissa Berthelot, and Guang-Zhong Yang

The Hamlyn Centre, Imperial College London, London SW7 2AZ, UK
c.bergeles@imperial.ac.uk

Abstract. Ophthalmoscopes have yet to capitalise on novel low-cost
miniature optomechatronics, which could disrupt ophthalmic monitoring
in rural areas. This paper demonstrates a new design integrating mod-
ern components for ophthalmoscopy. Simulations show that the optical
elements can be reduced to just two lenses: an aspheric ophthalmoscopic
lens and a commodity liquid-lens, leading to a compact prototype. Cir-
cularly polarised transpupilary illumination, with limited use so far for
ophthalmoscopy, suppresses reflections, while autofocusing preserves im-
age sharpness. Experiments with a human-eye model and cadaver porcine
eyes demonstrate our prototype's clinical value and its potential for ac-
cessible imaging when cost is a limiting factor[1].

1 Introduction

Given the extensive worldwide population suffering from a potentially blinding
ophthalmic pathology, innovation on intraocular observation methods is impera-
tive. In rural societies, patients that suffer from detectable and treatable diseases,
such as cataracts or retinopathy of prematurity, would benefit from easily ac-
cessible digital ophthalmoscopes. Notably, 80% of blindness is preventable when
detected early [1]. Disruptions in the miniaturisation of lenses, electronics, and
mechanical components, together with ubiquitous computing through micropro-
cessors, should instigate developments in ophthalmoscopy and reshape a field
substantially based on 20th century developments [2].

Retinal fundus imaging is a critical task in ophthalmoscopy, and, thus, the
focus of recent device innovations. Examples of new approaches to fundoscopy
mainly make use of smartphone technologies [3–5]. Initial approaches in 2012 en-
tailed observing the retina using a smartphone's camera and a handheld indirect
ophthalmoscopy lens [3]. Apart from leveraging the smartphone's camera, this
approach did not deviate from the principles of direct observation. The design
was improved in 2014 using a 3D-printed smartphone-attached length-adjustable
"arm" to hold the lens [5]. It was found that this approach was also cumbersome
to use due the requirement for manual mechanical focusing.

---

[1] With partial Fight for Sight, UK, support. Online resources: http://goo.gl/lvYbPp
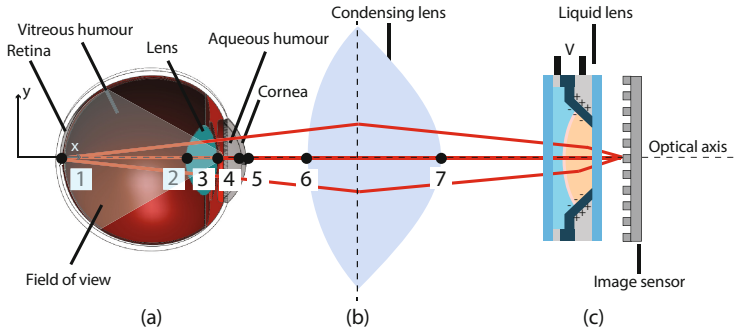
Fig. 1. Indirect ophthalmoscopy entails the use of a condensing lens, (b), held in front of the eye, (a). The image created by the lens is captured either with the clinician's eye, or, in our prototype, with a liquid lens and an image sensor, (c). The optical parameters of surfaces 1-7 are given in Table 1.

A limiting factor of smartphone-based approaches is that they do not account for the expense of the device itself. Thus, the reported costs are misleading and may amount to the cost of a hand-held commercial digital ophthalmoscope. Furthermore, the fact that 90% of blind people live in low-income countries [6] is not considered. Their location should be examined together with the lack of smartphone penetration, *e.g.*, only 37% of population in China, and only 19% in Kenya owns a smartphone [7]. Contrary, truly widespread ophthalmoscopic screening will make use of ubiquitous technology, as "dumb" mobile phones, which represent exceptional penetration (*e.g.*, 82% in Kenya [7]).

Our motivation is to use new lens technology to bring 21$^{\text{st}}$ century retinal imaging to vision care in developing economies, creating a low-cost digital ophthalmoscope that makes no use of a smartphone while minimising the system's optical and mechanical elements. Our device is based on state-of-the-art aspheric lenses and is among the first that uses liquid lenses. Optics simulations, selection of illumination components, and reflection-removal via relatively unexplored, in ophthalmoscopy, circularly polarised light, are described together with the selection of the appropriate autofocusing algorithm. Finally, the performance is evaluated with experiments in a human-eye phantom and porcine eyes.

2   Simulation, Design, and Integration

This section presents simulations, components, and integration of the developed digital ophthalmoscope with autofocusing software.

2.1   Optics

The human eye comprises the optical elements that create images on the curved retinal surface [see Fig. 1(a)]. Indirect digital retinal imaging is typically performed

through a series of lenses, starting with a high-magnification lens, termed condensing lens, held in front of the eye [see Fig. 1(b)]. This lens reduces the refractive effect of the eye and creates a retinal image. Subsequently, in conventional ophthalmoscopes, field lenses flatten this image for capture by the image sensor [see Fig. 1(c)]. Each lens increases device cost and size and requires additional light intensity since each lens causes reflections and scattering.

Advanced machining techniques have recently enabled the manufacturing of double aspheric lenses, *i.e.*, precisely manufactured lenses whose surface is described by high-order polynomials:

$$x = \frac{y^2/R}{1 + \sqrt{1 - ((c+1)y^2/(R^2)}} + a_4 y^4 + a_6 y^6 + a_8 y^8 + a_{10} y^{10} \qquad (1)$$

where R is the radius of curvature, c is the conic constant, a_{4-10} are the asphericity coefficients, and the axes x and y are shown in Fig. 1. In theory, this class of lenses removes the optical aberrations of the human eye and create flat images. They are hand-held under direct clinical retinal observation with slit lamps and additional ophthalmoscopy equipment.

Biometric eye models based on human population averages have been created to enable optics' optimisation for ophthalmoscopy. This paper bases its results on Navarro's wide-field eye [8], which is an established biometric model explaining the eye's optical aberrations in a large ($\sim 70°$, measured from the eye's centre) field-of-view [see Fig. 1(a)]. The biometric model and aspheric condensing lens parameters, based on [9], are given in Table 1 for completeness. The double aspheric lenses listed in this paper belong to the family of lenses described in [10], which differ among themselves primarily on the field-of-view and magnification.

Simulations are performed using optical design software (OSLO and Trace Pro) from Lambda Research [see Fig. 2(a)]. Assuming that the system must focus on an intraocular range of distances spanning ±5 mm around the nominal retinal depth, it is simulated that the images are formed behind the condensing lens at ±3.5 mm around the focal length. This suggests that a single secondary optical element with a minimum range of focus of 7.0 mm, suffices to capture the retinal images created by this type of aspheric lenses. This leads to compact indirect ophthalmoscopy devices with only two optical elements.

Traditionally, focusing lenses are mechanically actuated. The addition of mechanical components, however, complicates device integration. Liquid-lenses, on the other hand, achieve focusing electrically through electrowetting [11]. The voltage applied on the lens regulates its shape, from concave to convex, and its focal length. The Varioptic Artic 416, retrieved from a Digitus Webcam (DA-708117), satisfies the low-cost criteria, and, with a working distance from 6 cm to infinity, covers the full extent of the simulated retinal image locations. The lens is controlled through our custom electronics, based on the Femtoduino® microcontroller and the Supertex HV892 liquid lens driver for voltage regulation.

The imaging sensor was extracted from Microsoft's LifeStudio® webcam, and was selected due to its reduced cost and high pixel density (720p HD). According to [12], retinal observation systems should have a pixel resolution of 50 per
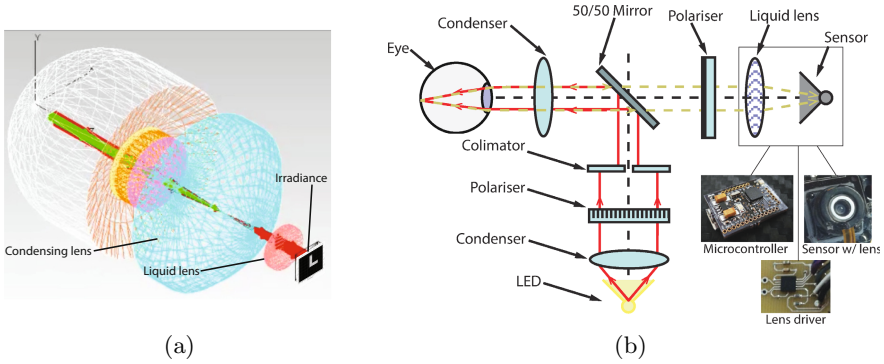
(a)   (b)

Fig. 2. (a) Simulation of optical elements and image sensor irradiance, and (b) Prototypical optical system schematics.

Table 1. Parameters of the optical system

Surface	Radius	Conic Constant	Thickness	Refractive Index
1	12.00 mm	0.00	16.32 mm	1.336
2	6.00 mm	-1.00	4.00 mm	1.420
3	-10.20 mm	-3.13	3.05 mm	1.337
4	-6.50 mm	0.00	0.55 mm	1.376
5	-7.72 mm	-0.26	3.11 mm	1.000
6	11.65 mm	-9.24	13.00 mm	1.523
7	-9.48 mm	-1.07	∞	
		Asphericity		
	a_4	a_6	a_8	a_{10}
6	4.078×10^{-5}	-1.542×10^{-7}	-2.647×10^{-9}	2.023×10^{-11}

degree. The selected sensor should be used in conjunction with a $\sim 30°$ field-of-view, *e.g.*, with a high magnification condensing lens for observing the macular area, such as the Digital High Mag® from Volk, Inc.. The assembly of the liquid-lens on the camera sensor is shown in Fig. 2(b).

2.2   Illumination

Ophthalmic observation is achieved via transscleral or transpupilary illumination. Diffused illumination through the sclera has been examined in the past by the authors and was found impractical due to scleral specularities and insufficient light intensity. Hence, the current prototype uses transpupilary illumination. Contrary to conventional Tungsten-lamp-based illumination, this new system uses high-power current-controlled LEDs (Luxon Rebel 4000K LED). Harmful UV-light can be filtered out using a UV-blocking-filter.

Transpupilary illumination suffers from reflections caused by the optical interfaces. These reflections are usually avoided with annuli that assign part of

the pupil for imaging and the rest for illumination, resulting in a reduced field of view. Alternatively, our prototype uses circularly polarised light whose application in ophthalmoscopy is relatively unexplored [13], and has not been used by any smartphone-based apparatus. Reflection removal is achieved by two perpendicularly crossed polarisers, one placed at the emission LED and one at the imaging sensor. Reflected light retains polarisation, and, hence, is blocked by the second polariser, which permits only the light backscattered from the retina. The reduction of the optical elements minimises light loss due to reflection, and, hence, allows the introduction of the polarisers without a harmful increase in the supplied light energy.

The complete optical schematic of the device is shown in Fig. 2(b). The polarised LED light passes through a condensing lens and a collimator/pinhole, and is reflected by a 45° beam-splitter/mirror (50/50) (beamsplitter plate) towards the ophthalmoscopic condensing lens, which focuses it on the retina. Backscattered light is collimated by the condensing lens, and, through the mirror and the liquid-lens, focuses on the image sensor. Co-axiallity of the components is achieved using a concentric tube approach, where each tube houses an optical element.

2.3   Software

The liquid-lens is driven using Arduino® firmware. The entire system is integrated with software that currently runs on Matlab®; communication is via USB. The software controls video recording, light-intensity control, and autofocusing. Autofocusing is based on adjusting the lens' focus to maximise image information. The user selects the image region to be kept in-focus.

Three common sharpness metrics of increasing complexity were considered: a) the Tenengrad variance, *i.e.* the variance of image gradient, b) the Laplacian variance, and c) the Wavelet variance, *i.e.*, the variance of frequency-enhanced wavelet-transformed images:

$$\delta_{xy,\text{tenengrad}} = \sum_{(i,j)\in\Omega(x,y)} \left(G(i,j) - \overline{G}\right)^2 \tag{2}$$

$$\delta_{xy,\text{laplacian}} = \sum_{(i,j)\in\Omega(x,y)} \left(L(i,j) - \overline{L}\right)^2 \tag{3}$$

$$\delta_{xy,\text{wavelet}} = \sum_{(i,j)\in\Omega(x,y)} \sum_{n\in L,H,m\in L,H} \left[\left(W_{nm}(i,j) - \overline{W_{nm}}\right)^2\right] \tag{4}$$

where (i,j) span the pixels of the selected region $\Omega(x,y)$, G is the magnitude of the image gradient, $\overline{G}$ the magnitude's average, L is the Laplacian's magnitude, $\overline{L}$ the average, and W_{LH}, W_{HL}, W_{LL}, and W_{HH} correspond to the respective low-and-high image frequency subtends of the wavelet transform (see [14] for details). Maximisation of the focus functions is related to stronger edge information, *i.e.* sharper, images. The computational performance of the sharpness calculations in relation with linear optimal-focus search and bisection search
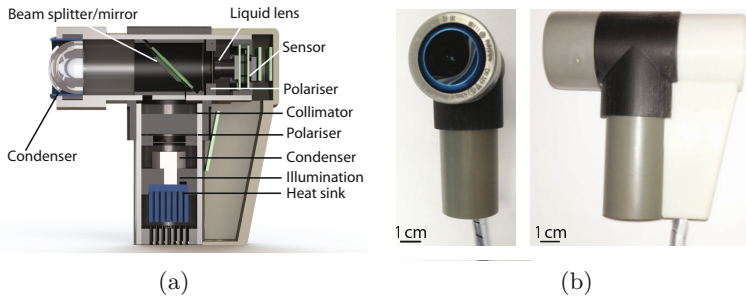
(a)   (b)

Fig. 3. (a) CAD with mechatronics components annotated, and (b) The prototype.

were evaluated. The linear search method exhaustively searches for the best in-focus image throughout the lens' focus range, thus avoiding local minima, while the bisection search method exploits the "bell-shaped" nature of the sharpness function to alternate its search around an estimated optimal focus position. Finally, autofocus is triggered only after loss of focus, *i.e.*, when the calculated focus-score for image region changes by more than a user-specified percentage.

3   Results

Figure 3 shows the actual device and the prototype's CAD with all mechatronics annotated. All housing components are 3D-printed on an Eden 350, with internal components printed in black to minimise light reflection. The prototype is evaluated with experiments in a human-eye phantom and porcine eyes.

3.1   Human Eye Phantom

The human eye phantom from Gwb International, Ltd., is air-filled and has a single lens that mimics the compound effect of the human eye optics. It's hand-painted retina makes it a common platform for ophthalmoscope demonstrations. Reflection removal and autofocusing are evaluated on this phantom.

Figure 4(a)-top demonstrates the extent of reflections without the polarisers. Removal of the reflections via software, as is commonly performed in medical image processing, would only lead to extended image areas with approximated information. The perpendicularly crossed polarisers dramatically reduce the reflections, as shown in Fig. 4(a)-bottom.

Autofocusing using the Tenengrad, Laplacian, and Wavelet variances is evaluated by discretising the range of focus, *i.e.*, the liquid-lens control voltage, into 255 levels, and comparing the selected focus-score maxima. In the representative example of Fig. 4(b), it can be seen that the focus-score functions lead to similar results. Our experiments showed that the Tenengrad variance requires only 4.9 s for a complete focus sweep, compared to 7.4 s for the Laplacian variance and 12.1 s for the Wavelet variance. Hence, the computationally simpler Tenengrad
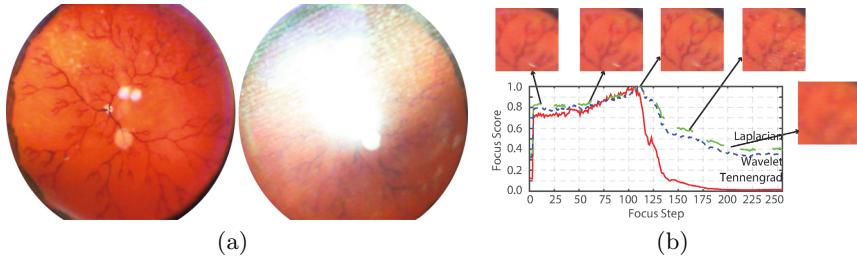
(a)   (b)

Fig. 4. (a) Reflections on the eye phantom without (left), and with (right), polarisation, and (b) example of focus-point estimation for the three focus-score functions.
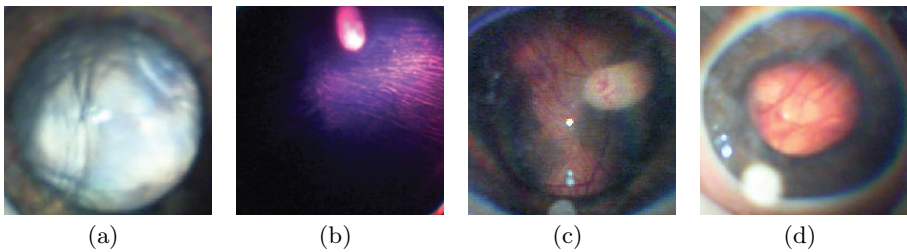

(a)   (b)   (c)   (d)

Fig. 5. Retinal fundus imaging in cadaver porcine eyes. (a) Opaque intraocular lens, (b) retinal haemorrhage, (c), (d) additional retinal images.

focus metric was selected. In addition, the linear search method outperformed the bisection-search method due to the fact that the liquid lens' limited response bandwidth cannot follow the rapid changes in voltage required by the later. Also, the linear sweep avoids local minima. In practice, we sweep the focus range in tuneable steps (every 9 voltage steps, specifically, as decided with preliminary experiments) to achieve faster refocusing; the speed could be further improved by searching in the vicinity of the previous best focus position.

3.2 Ex Vivo Experiments

Porcine eyes are a good model of human eyes in terms of dimension and optical components, so they are routinely used for training. Fresh porcine cadaver eyes were purchased and transported to our lab in ice. During experiments with 20 porcine eyes, the corneas were moisturised to avoid opacification. Since the pupil of the cadaver eyes is relaxed, the intraocular field of view is reduced. Autofocusing is achieved by maximising the Tenengrad measure of a window at the centre of the image.

The ophthalmoscope was used by a clinical student to study the porcine retinas. Figure 5(a) shows an opacified intraocular lens that could indicate cataract. Such examinations are especially useful for rural populations. In Fig. 5(b)-(d), the retina is in focus; extended field of view could be visualised by moving the

eye. A pathological case was identified among the porcine samples: Fig. 5(b) shows a haemorrhage resulting in the dark purple colour in the retinal image. Hence, the clinical value of this low-cost device is experimentally supported.

4   Conclusions and Discussion

Routine retinal observations are paramount for disease prevention, and novel optomechatronics support the ophthalmoscope's evolution. Our primary contributions include the integration of a liquid lens and an aspheric lens with cross polarising filters, and autofocusing in a compact device. Its clinical value is supported by *ex vivo* experiments, and its low-cost, $200 excluding the necessary aspheric lens, makes it accessible to developing economies. Ongoing work investigates image improvement and focus estimation on an embedded chip.

References

1. Pascolini, D., Mariotti, S.P.: Global estimates of visual impairment: 2010. British J. Ophthalmology 300538, 1–5 (2011)
2. Keeler, C.R.: A brief history of the ophthalmoscope. Optometry in Practice 4, 137–145 (2003)
3. Bastawrous, A.: Smartphone fundoscopy. Ophthalmology 119(2), 432–433 (2012)
4. Giardini, M.E., Livingstone, I.A.T., Jordan, S., Bolster, N.M., Peto, T., Burton, M., Bastawrous, A.: A smartphone based ophthalmoscope. In: IEEE Int. Conf. Engineering in Medicine and Biology, pp. 2177–2180 (2014)
5. Lin, S.J., Yang, C.M., Yeh, P.T., Ho, T.-C.H.: Smartphone fundoscopy for retinopathy of prematurity. Taiwan J. Ophthalmology 4(2), 82–85 (2014)
6. Bastawrous, A., Hennig, B.D.: The global inverse care law: a distorted map of blindness. British J. Ophthalmology 96, 1357–1358 (2012)
7. Bolster, N.M., Giardini, M.E., Livingstone, I.A.T., Bastawrous, A.: How the smartphone is driving the eye-health imaging resolution. Expert Review on Ophthalmology 9(6), 475–485 (2014)
8. Escudero-Sanz, I., Navarro, R.: Off-axis aberrations of a wide-angle schematic eye model. J. Optical Society of America A 16(8), 1881–1891 (1999)
9. Bergeles, C., Shamaei, K., Abbott, J.J., Nelson, B.J.: Single-camera focus-based localization of intraocular devices. IEEE Trans. Biomedical Engineering 57(8), 2064–2074 (2010)
10. Volk, D.A.: Indirect ophthalmoscopy lens for use with split lamp or other biomicroscope, January 6, 1998. U.S. Patent 5,706,073
11. Kuiper, S., Hendriks, B.H.W.: Variable-focus liquid lens for miniature cameras. Applied Physics Letters 85(7), 1128–1130 (2004)
12. Bernardes, R., Serranho, P., Lobo, C.: Digital ocular fundus imaging: a review. Ophthalmologica 226(4), 161–181 (2011)
13. Tran, K., Mendel, T.A., Holbrook, K.L., Yates, P.A.: Construction of an inexpensive, hand-held fundus camera through modification of a consumer point-and-shoot camera. Investigative Ophthalmology and Visual Science 53(12), 7600–7607 (2012)
14. Yang, G., Nelson, B.J.: Wavelet-based autofocusing and unsupervised segmentation of microscopic images. In: IEEE/RSJ Int. Conf. Intell. Rob. Sys., pp. 2143–2148 (2003)